Optical properties of MgH_2 measured *in situ* by ellipsometry and spectrophotometry

J. Isidorsson,[1,*] I. A. M. E. Giebels,[1,†] H. Arwin,[2] and R. Griessen[1]
[1]*Faculty of Sciences, Department of Physics and Astronomy, Condensed Matter Physics, Vrije Universiteit, De Boelelaan 1081, 1081 HV Amsterdam, The Netherlands*
[2]*Laboratory of Applied Optics, Department of Physics and Measurement Technology, Linköping University, SE-581 83 Linköping, Sweden*
(Received 18 May 2003; published 29 September 2003)

The dielectric properties of α-MgH_2 are investigated in the photon energy range between 1 and 6.5 eV. For this purpose, a sample configuration and experimental setup are developed that allow both optical transmission and ellipsometric measurements of a transparent thin film in equilibrium with hydrogen. We show that α-MgH_2 is a transparent, color neutral insulator with a band gap of 5.6 ± 0.1 eV. It has an intrinsic transparency of about 80% over the whole visible spectrum. The dielectric function found in this work confirms very recent band-structure calculations using the GW approximation by Alford and Chou (unpublished). As Pd is used as a cap layer we report also the optical properties of PdH_x thin films.

DOI: 10.1103/PhysRevB.68.115112 PACS number(s): 78.20.Bh, 77.55.+f, 77.22.Ch, 78.66.Nk

I. INTRODUCTION

Among metal hydrides[1] the magnesium hydrogen system has always occupied a special place. Magnesium reacts reversibly with hydrogen to form MgH_2. It is thus considered to be one of the most important candidates for the reversible storage of hydrogen[2] due to its lightweight, low cost, and high hydrogen storage capacity (7.6 wt% of hydrogen). In spite of the large number of publications on Mg-MgH_2 only little is known about the intrinsic physical properties of this system. The scarcity of data for MgH_x is mainly due to the experimental difficulties encountered when trying to hydride Mg.[3] Nowadays, a great effort is made to improve the hydrogen absorption/desorption kinetics by making nanocrystalline Mg (Ref. 4) and/or adding, e.g., transition metals[5–7] by ball milling.

Recent theoretical calculations[8] reproduce that MgH_2 undergoes various phase transitions[9,10] as a function of pressure. All theoretical calculations published so far[8,11–13] [using either the local-density approximation (LDA) or the generalized gradient approximation (GGA)] predict band gaps between 3.1 and 4.2 eV for α-MgH_2. This is smaller than the few sporadic experimental values reported until now. Krasko[14] mentions a value of 5.16 eV for the band gap from unpublished work by Genossar. He and Pong[15] determined in an indirect way using Penn's formula[16] an average band gap of 5.8 eV. Yamamoto *et al.*[17] report an optical transmission spectrum for a thin film in which the transmission vanishes at 6.05 eV (205 nm). Apart from that Ellinger *et al.*[18] found an index of refraction of 1.95 and 1.96 for the ordinary and extraordinary rays at 589.3 nm. The dielectric properties have not been studied at all. This triggered our interest to study the optical properties of MgH_2 in detail.

Another strong reason for our interest in MgH_2 stems from metal-hydride switchable mirrors. In 1996 Huiberts *et al.*[19] discovered that Y and La thin films change reversibly from shiny, metallic films to transparent, insulating films upon hydrogenation either by changing the surrounding hydrogen gas pressure or the electrolytic cell potential.[20,21] In 1997 van der Sluis *et al.*[22] discovered that all rare-earth (RE) metals exhibit such a switchable behavior. However, all these materials have a characteristic color in the fully hydrogenated state because their band gap is in the visible part of the optical spectrum ($E_g < 3$ eV). They showed that alloying with Mg results in color neutral switchable mirrors. This is very important for applications in, e.g., ''smart'' windows. In 2001 Richardson *et al.*[23] reported that Mg_zNi ($z \geqslant 2$) also features reversible switching behavior upon hydrogenation. In all these cases (RE-Mg and Mg_zNi), the band gap is shifted to higher energies with increasing magnesium concentration.[22–26] Furthermore, all these alloys disproportionate upon hydrogenation.[24,27–29] This disproportionation is also known for bulk RE-Mg.[30,31] The available data suggest that the shift of the band gap to higher energies is due to the formation of MgH_2 which is expected to have a large band gap. At the same time the reflectance in the low hydrogen phase (when the sample is unloaded) increases due to Mg which has a high reflection.[22,32] At intermediate concentrations the coexistence of Mg and MgH_2 seems to play an important role in the realization of a highly absorbing, black state that is observed during loading and unloading of RE-Mg alloys.[33,34] It may also play a role in the black state observed in Mg_zNiH_x.[35] Thus, to understand the role of MgH_2 in Mg-containing switchable mirrors it is essential to determine the optical properties of MgH_2 thin films.

In this paper we study thin films of magnesium hydride with spectrophotometry and ellipsometry and determine the dielectric function and the optical band gap. For this purpose we use a special substrate geometry and a special type of optical gas loading cell.

II. EXPERIMENT

MgH_2 thin films are made in two steps. First Pd capped metallic Mg films are deposited under UHV conditions on an appropriate substrate. The Pd cap layer is necessary to protect Mg against oxidation and to promote hydrogen dissociation and absorption. The films are subsequently loaded with hydrogen under high pressure up to the composition MgH_2.

The hydrogenation of Mg to MgH_2 is, however, not

 ©2003 The American Physical Society

straightforward as was shown by Krozer, Kasemo, and others.[36–40] Palladium capped Mg films exhibit unusual kinetics due to the formation of a blocking MgH_2 layer at the interface between Pd and Mg. The MgH_2 layer prevents H to diffuse[41] to the metallic Mg that is still present underneath. The formation of this blocking layer can be circumvented by starting hydrogenation at relatively low (1 mbar) H_2 pressure at a temperature of 100 °C. Magnesium films with thicknesses up to 150 nm can be fully transformed to MgH_2 in this way.[38,42]

A. Film deposition

Thin, polycrystalline films of Mg and Pd are deposited at room temperature in an UHV molecular-beam epitaxy system with a background pressure of 10^{-9} mbar, using material of 99.9% purity. The magnesium films are evaporated from a Knudsen cell and covered with a Pd cap layer. These palladium films are deposited from an e-beam evaporation unit. Typically, we deposit films simultaneously on a 10×10 mm^2 glassy carbon substrate for Rutherford backscattering spectrometry (RBS), 10×10 mm^2 quartz substrates for x-ray diffraction, resistivity and/or atomic force microscopy measurements, and on a quartz substrate (Ø 42 mm, Heraeus Suprasil 1) for optical measurements.

B. Film characterization

RBS is used to determine possible contamination of the films. For this glassy carbon substrates are used in order to separate the Mg signal from the background signal of the substrate. An oxygen contamination between $0.03\leqslant[O]/[Mg]\leqslant0.085$ has been found.

The thickness of the film is measured with a DekTac[3] or a Tencor Alpha step 200 mechanical stylus profilometer. The surface structure, both before and after hydrogen loading, is investigated with a NanoScope III atomic force microscope (AFM), operating in tapping mode using silicon cantilevers. The scanned areas are typically 1×1 and 5×5 μm^2 from which the root-mean-square (rms) roughness is determined. The thickness and roughness values from these techniques are used as input parameters in the modeling of the transmission, reflection, and ellipsometric data (see Sec. III).

Some samples are contacted ultrasonically with four 30-μm aluminum wires to monitor the resistivity with the van der Pauw method[43] during loading with hydrogen.

X-ray experiments are carried out with Cu-K_α radiation in a Rigaku ''Rotaflex'' RU 200 or Bruker D8 Discover x-ray diffractometer to monitor the transformation of hcp Mg to rutile MgH_2 in a θ-2θ mode.

C. Optical techniques

Optical reflection and transmission measurements at room temperature (RT) are carried out in a Perkin Elmer Lambda 900 spectrophotometer in the range $0.5<\hbar\omega<6.7$ eV $(2500>\lambda>185$ nm). The specular and total transmission is recorded while the spectrophotometer is purged with argon or nitrogen in order to reduce absorption by O_2 in the ultraviolet (UV) and H_2O in the infrared. The quartz substrates (without film) and Pd samples are measured in reflection geometry from the top side (i.e., the metallic side) at near normal incidence (8°) in an absolute reflection unit.

Ellipsometry measurements (at RT) in the energy range 1.0–6.5 eV $(1240>\lambda>190$ nm) are carried out in a rotating analyzer variable-angle spectroscopic ellipsometer (VASE, J.A. Woollam Co. Inc.), using the WVASE32 software program for data acquisition and analysis. This instrument measures the ratio of the complex Fresnel reflection coefficients R of parallel (p) and perpendicular (s) polarized light.[44] This ratio defines the ellipsometric angles $\Psi(\omega)$ and $\Delta(\omega)$ according to

$$\frac{R_p}{R_s}=\tan[\Psi(\omega)]\exp[i\Delta(\omega)]. \tag{1}$$

Three angles of incidence (60, 65, and 70°) are used to obtain adequate sensitivity over the whole spectral range. Ellipsometric data (Ψ,Δ) are recorded at each data point as an average of at least 100 and up to 4000 revolutions of the analyzer for the most critical data.

D. Semicylindrical substrate

As the Pd cap layer on top of the very transparent MgH_2 layer is strongly absorbing, ellipsometry cannot be carried out from the Pd side. Thus, ellipsometry measurements need to be performed from the ''backside,'' through the substrate. Flat substrates would need to be so thick that reflections from the front and backside of the substrate can be well separated. With a 2 mm diameter of the light beam the substrate must be thicker than 3 mm. However, at large angles of incidence the intensity loss in the light beam is substantial due to reflections at the air/substrate interface. Furthermore, at energies close to the limit of the ellipsometer (6–6.5 eV), the intensity of the light beam is diminishing quickly. These limitations can be avoided with a semicylindrical substrate.

This substrate is designed for normal incidence of light at the ambient/substrate interface and oblique incidence at the internal substrate/MgH_2 interface (see Fig. 1). For the normal incident approximation to be valid, the diameter of the semicylindrical substrate must be large compared to the size of the light beam (2 mm). For practical reasons we choose a semicylindrical substrate with a diameter of 42 mm. The top part of the semicylindrical substrate is cut away parallel to the base surface to enable transmission measurements. This design allows the angle of the incident light onto the sample to vary between 55° and 75° from the normal. Both the flat and the semicylindrical substrates are made of quartz glass (Heraeus Suprasil 1). This material is transparent deep into the UV beyond the limit of our ellipsometer and spectrophotometer.

On the top of the large flat face we deposit, under exactly the same condition, three films with different Mg thicknesses (see Fig. 1). This allows us to analyze compositionally identical films. This method makes the determination of the dielectric function from ellipsometric data more reliable.[45,46]

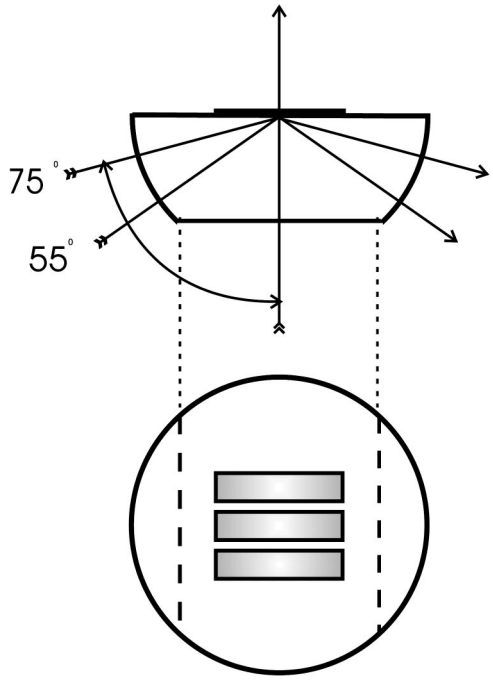

FIG. 1. Semicylindrical quartz glass substrate for ellipsometry and transmission measurements. The upper figure is a side view of the substrate, the one on the bottom a top view. A perspective view is given in Fig. 2. The angle of incidence of light can be varied between 55 and 75°. On the flat part of the substrate three samples with different Mg thicknesses are deposited. They are all covered with a 12-nm-thick Pd cap layer.

E. Optical gas loading cell and high-pressure loading chamber

In order to measure the optical properties of MgH_2 and PdH_x *in situ* in equilibrium with hydrogen at various pressures, we designed an experimental setup consisting of three parts: (i) a substrate/window (see Fig. 1), (ii) an optical gas loading cell, and (iii) a high-pressure loading chamber. Components (ii) and (iii) are described below in more detail. The setup also includes a special substrate holder with a sliding mask for the deposition of the films and a holder to attach the optical gas loading cell to the ellipsometer.

A semicylindrical or a flat substrate with the Pd-capped MgH_2 films deposited on top functions as window in the optical gas loading cell (see Fig. 2). For ellipsometry the sample/window is illuminated through the substrate to measure the backside of the film. For *in situ* transmission measurements a window is mounted on the opposite side of the cell as well. The sample can be exposed to a controlled hydrogen gas atmosphere during the measurements via two tubes connected to a vacuum pump and hydrogen gas cylinder. The cell is designed for vacuum, but works also reliably up to a few bar hydrogen pressure.

As already mentioned in the introduction of Sec. II, hydrogenation of Mg to MgH_2 can be successfully achieved at moderate temperatures (100 °C) by starting at low hydrogen pressure.[38,42] Therefore, to be sure that our thin films of Mg are completely transformed to MgH_2 we start loading with a H_2 pressure of 1 mbar and increase it in steps (within a few hours) up to 100-bar H_2. To do this the optical gas loading cell is mounted inside a high-pressure loading chamber. This chamber is made of stainless steel and proof pressurized to 200 bar. The design is such that it is not necessary to expose the sample to the ambient after loading at 100-bar H_2. It is, namely, possible to release hydrogen and close the optical gas loading cell when a pressure of 1-bar hydrogen or less is reached before disconnecting it from the high-pressure chamber. This high-pressure chamber is also equipped with an electrical feed through with several wires to permit measurements of the resistivity of a sample during hydrogenation and of the temperature inside the chamber with a RhFe100 sensor. During hydrogen loading of a Mg film the total chamber can be resistively heated up to 100 °C.

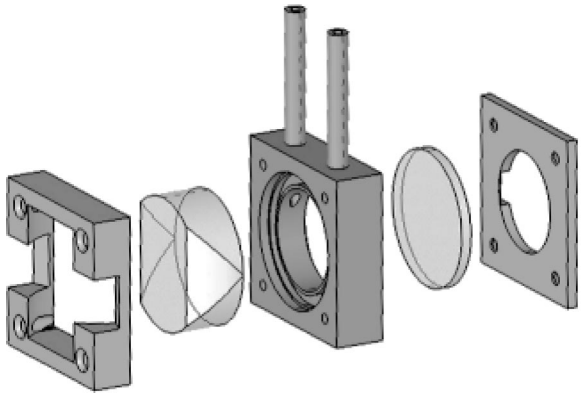

FIG. 2. Exploded view of the optical gas loading cell for *in situ* ellipsometry and transmission measurements in a hydrogen environment. In this sketch the cell is shown with the semicylindrical substrate (see Fig. 1) as sample window at the front side. Alternatively, a flat window such as the one at the backside of the cell can be used as sample substrate.

III. RESULTS

A. Sample characterization

Since Mg is a metal and MgH_2 an insulator, the time evolution of hydrogenation can be followed *in situ* in real time by monitoring the change of the resistivity.[47] This allows us to optimize the hydrogen pressure (starting at low pressures and increasing it stepwise to 100-bar H_2) in such a way that no impenetrable MgH_2 layer is formed at the interface between Pd and Mg. For practical reasons we have mounted an extra sample in the high-pressure loading chamber for resistivity measurements.

The resistivity of this as-deposited 150-nm Mg film covered with 15 nm of Pd at RT is 6.5 $\mu\Omega$cm [the literature value for bulk Mg at 20 °C is 4.4 $\mu\Omega$cm (Ref. 48)]. The reflection of this as-deposited film is high in the visible and near-infrared regions ($\sim$80%). Both the low resistivity and the high reflection indicate the good quality of the film. After loading the resistivity reaches 680 $\mu\Omega$cm under 100-bar H_2 at 100 °C. Since MgH_2 is an insulator one would at first sight expect a much higher value. The moderate resistivity found experimentally is, however, due to the metallic Pd cap

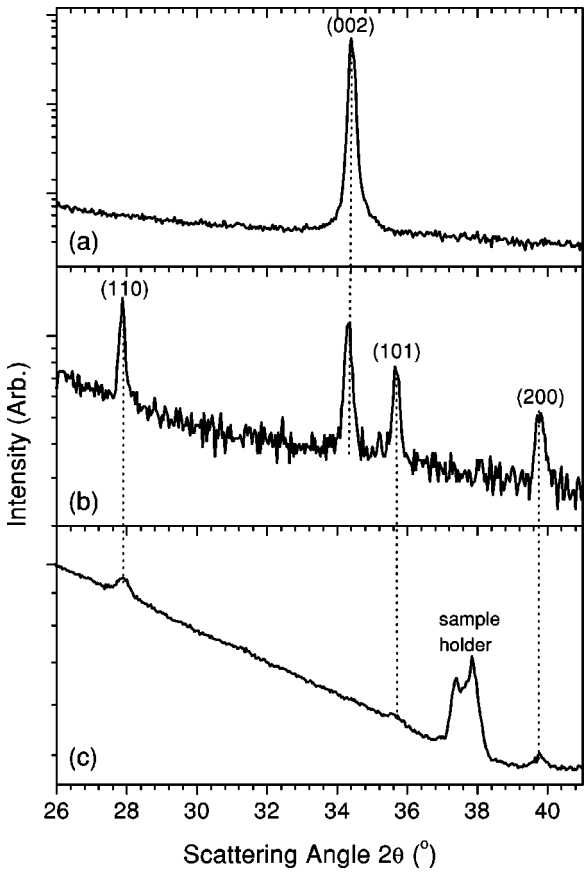

FIG. 3. X-ray-diffraction spectra of a 188-nm Mg/10-nm Pd film (a) as deposited, (b) loaded up to 1-bar H_2, and (c) of a 150-nm Mg/15-nm Pd film loaded up to 100-bar H_2. The large background is due to the quartz substrate.

layer that shortcuts the MgH_2 layer. Moreover, at a temperature of 100 °C, Mg and Pd may interdiffuse to form a Mg-Pd alloy.[39,49] This intermixing has been suggested for Pd capped Y as well,[50] and was conclusively shown with photoelectron spectroscopy recently.[51] RBS showed an intermixing of Mg and Pd in our films as well. This can be due to either alloying, interface roughening, or both. The net result is that a relatively Pd-rich Pd-Mg alloy is formed on top of MgH_2 that absorbs some hydrogen but does not become insulating and this causes the shortcut.

In the as-deposited metallic state, hcp Mg has a preferential growth direction, and only the (002) reflection is present in the x-ray diffractogram [see Fig. 3(a)]. Loading a thin Mg film in 1-bar H_2 at 100 °C does not transform Mg completely to MgH_2 [see Fig. 3(b)]. Loading at 100 bar and 100 °C, on the other hand, left no traces of metallic Mg. Only the peaks corresponding to the tetragonal structure of the rutile type[18] of α-MgH_2 are observed [see Fig. 3(c)]. Such a preferred growth direction is not observed for MgH_2 where weak signals from the (110), (101), and (200) peaks can be seen. Rocking curves around the (002) Mg peak and the (110) MgH_2 peaks show that our samples are polycrystalline.

AFM measurements revealed a significant difference between the as-deposited Pd covered Mg film and the fully hydrogenated films (see Fig. 4). Mg expands by 32% in volume when transforming from hcp Mg to rutile MgH_2.[52] Since the film is clamped by the substrate it cannot expand laterally and all the expansion must take place out of plane. With AFM we indeed noted an increase in the rms roughness from 5 nm to 14 nm. It can be seen as well that our top layer of Pd is not fully covering the Mg layer below. With a mechanical stylus profilometer we found a corresponding increase of the thickness of the film from 113 to 162 nm. This 43% increase is larger than the expected 32% volume expansion because the mechanical stylus has a tip radius of 12.5 μm, and hence cannot probe the deep valleys seen on the AFM image. During ellipsometry we look through the substrate at the backside of our films and not from the top side as with AFM. Nevertheless, we found that surface roughening needed to be taken into account when modeling the ellipsometric data.

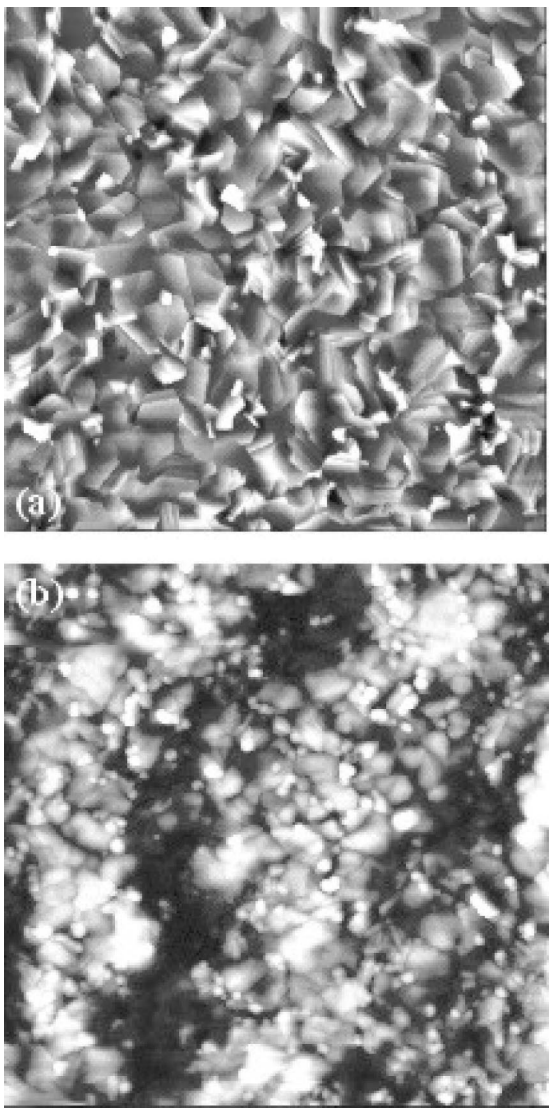

FIG. 4. AFM images of the surface (5×5 μm^2) of a 101-nm Mg/12-nm Pd (a) as deposited and (b) after loading with hydrogen at 100-bar. The root-mean-square roughness increases from 5 to 14 nm due to the 32% volume expansion accompanied by the transition from hcp Mg to rutile MgH_2.

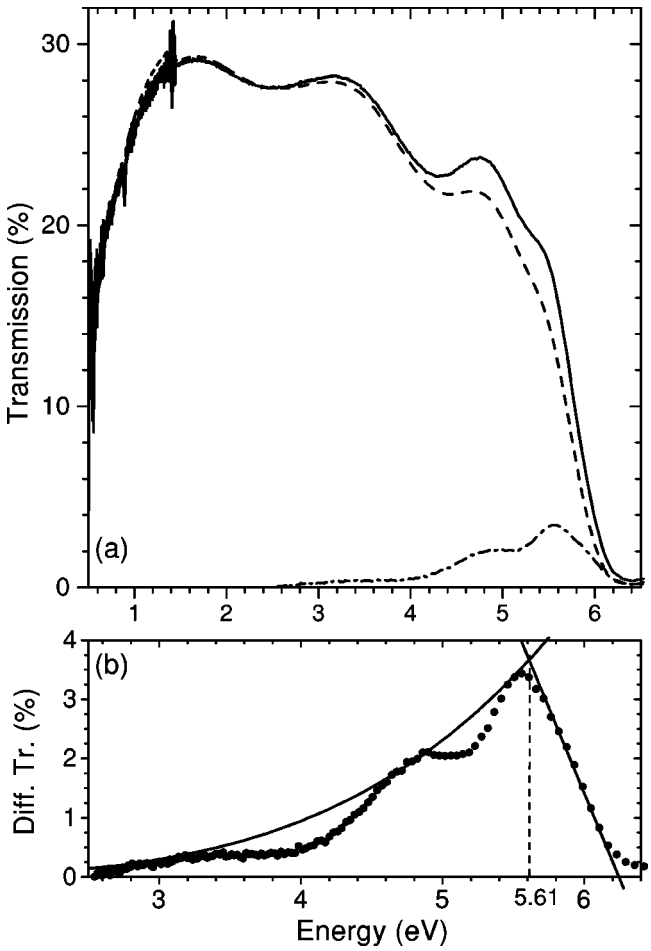

FIG. 5. (a) Total (solid line), specular (dashed line), and diffuse (dashed dotted line) transmission as a function of photon energy for a 150-nm-thick MgH_2 film capped with 12-nm Pd and loaded at 100 °C in 100 bar of hydrogen. (b) Detail of the diffuse transmission. A fit using Eq. (2) and an extrapolation of the transmission edge are shown. The intersection of these two curves gives an estimate of 5.61 eV for the optical band gap.

B. Transmission and band gap of MgH_2

The optical transmission of Pd capped MgH_2 films is measured *in situ* in 1-bar H_2 using the gas loading cell (see Fig. 2). Figure 5 shows the total, specular, and diffuse transmission of a 150-nm-thick MgH_2 film capped with 12-nm Pd, loaded at 100-bar H_2 and 100 °C. The total transmission is measured with the optical gas loading cell placed at the entrance port of the integrating sphere in the spectrophotometer. In this experiment a flat 3-mm-thick quartz glass substrate is used. Since we look at our film from the substrate side, the MgH_2 layer is situated 3 mm away from the port of the integrating sphere. The specular transmission is measured with the sample in the sample compartment, using the direct detector to monitor the signal. The difference between these two signals is the diffuse (scattered) transmission. It is probably due to the rough surface [see Sec. III A and Fig. 4(b)] of our loaded samples. This diffuse transmission T_d has a strong wavelength dependence and is proportional to

$$T_d \propto \frac{1}{\lambda^4} \propto (\hbar\omega)^4, \tag{2}$$

where λ is the wavelength of light.[53] It is clear from Fig. 5(b) that the diffuse transmission decreases strongly above the band gap as the film starts to absorb light. The optical band gap E_g can be estimated from the intersection of a fitted $(\hbar\omega)^4$ curve to the data and an extrapolation of the flank of the absorption edge. Using this so-called "Rayleigh method" we find $E_g = 5.61$ eV for this sample and $E_g = 5.67$ eV for a second sample.

Another estimate for E_g can be obtained from the absorption edge of the transmission spectra using the Lambert-Beer law, $T(\omega) = T_0 \exp[-\alpha(\omega) d]$, where α is the absorption coefficient, d is the film thickness, and T_0 contains the transmission of the Pd cap layer and the quartz substrate. In the region of the absorption edge, T_0 can be considered as constant in our films (see Fig. 8). According to Tauc, the frequency dependence of α near the band edge is related to the optical gap through[54,55]

$$\alpha(\omega) \propto \frac{(\hbar\omega - E_g)^\nu}{\hbar\omega}. \tag{3}$$

For direct, allowed (forbidden) transitions $\nu = \frac{1}{2}$ ($\nu = \frac{3}{2}$) and for indirect, allowed (forbidden) transitions $\nu = 2$ ($\nu = 3$). In amorphous material it has been found that $\nu = 2$ gives the best results. Combining these equations gives

$$\ln T(\omega) = \ln T_0 - C \frac{(\hbar\omega - E_g)^\nu}{\hbar\omega}. \tag{4}$$

The constants $\ln T_0$, C, and E_g are determined from a fit to the transmission spectra near the absorption edge in the interference-free region (>5.4 eV).

Applied to the total transmission this "Tauc procedure" gives a gap of 5.48 ± 0.05 eV using $\nu = 2$. It was also possible to get a Tauc fit with $\nu = 3$ and $\nu = \frac{3}{2}$. However, using $\nu = 3$ gives values that are too low compared to the "Rayleigh procedure" and we might be fitting an interference fringe instead of the absorption edge. For $\nu = \frac{3}{2}$ the quality of the fit is not as good and we obtain a gap of 5.75 ± 0.05 eV from the total transmission.

Since the diffuse transmission increases rapidly at small wavelengths (i.e., with increasing energy), it is clearer where the absorption starts in this spectrum than in the total transmission. Therefore, we conclude that the band gap of MgH_2 is 5.6 ± 0.1 eV.

C. Ellipsometry

1. Modeling strategy

Extracting the dielectric function of a layer from ellipsometric data on samples like ours, which consists of several thin layers on a substrate, is a complex task. The complicated inversion of the ellipsometric data to the dielectric function is, however, greatly simplified if the optical properties of

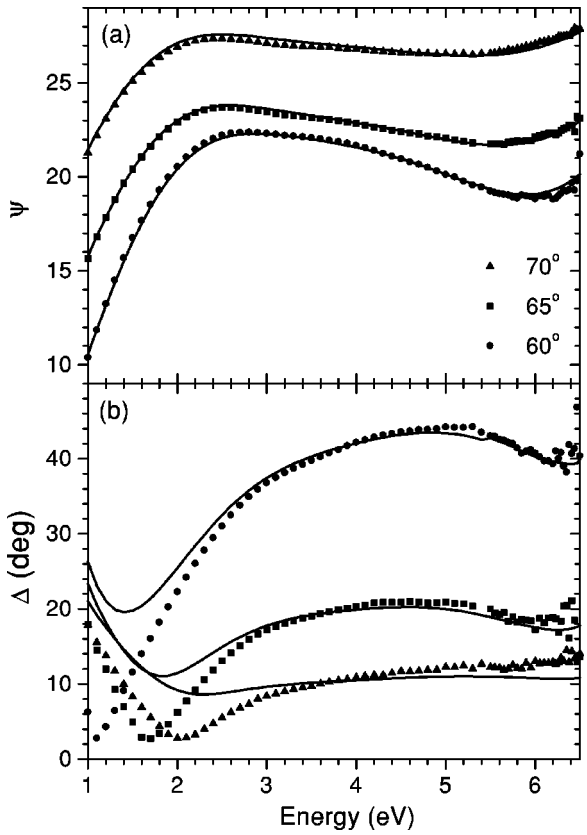

FIG. 6. Experimental and fitted ellipsometric data, Ψ (a) and Δ (b) for a 12-nm-thick Pd film in 1-bar H_2 used to determine the dielectric function of PdH_x (see Fig. 8). The mean-squared error corresponding to the fit is 7.4.

each individual layer is measured in separate experiments. For this reason we adopted the following strategy to determine the dielectric function of MgH_2.

We start by investigating the dielectric properties of the quartz substrate. The second step is to evaluate the optical properties of the hydrogenated Pd cap layer. This is done by investigating a 12-nm-thick film of Pd on quartz, hydrogenate it in 1-bar H_2 using the optical gas loading cell and measure it in the ellipsometer. In a third step we study the properties of the hydrogenated interface region between Pd and MgH_2 carefully since earlier experiments with Mg-Pd thin films showed that interdiffusion starts already at 100 °C.[39,49] This is done by investigating a ''Pd-Mg'' alloy layer consisting of 10-nm Mg on a quartz substrate covered with 10-nm Pd. This sample is loaded with hydrogen at 100 °C and 100 bar and measured in the ellipsometer. The final step is to measure the total stack (quartz, MgH_2, Pd-Mg) and to extract the optical properties of MgH_2 using the optical properties of all the other layers.

An optical model is defined for each sample and in the fitting procedure the difference between the calculated (cal) and the measured (exp) (Ψ,Δ) values (see Sec. II C) are weighted with the experimental standard deviation σ and fitted with a Levenberg-Marquardt algorithm to minimize the mean-squared error ξ^2 according to[56,57]

$$\xi^2=\frac{1}{2N-M}\sum_{\lambda}\sum_{\Theta}\left\{\left[\frac{\Psi_{\lambda,\Theta,\mathrm{cal}}-\Psi_{\lambda,\Theta,\mathrm{exp}}}{\sigma_{\lambda,\Theta,\Psi}}\right]^2+\left[\frac{\Delta_{\lambda,\Theta,\mathrm{cal}}-\Delta_{\lambda,\Theta,\mathrm{exp}}}{\sigma_{\lambda,\Theta,\Delta}}\right]^2\right\}, \quad (5)$$

where N is the number of (Ψ,Δ) pairs, M is the number of fitting parameters, and the indices λ and Θ denote data points at different wavelengths and angles. In most cases also normal-incidence transmission data, T, are used to improve the accuracy of the determination of the dielectric function.[58] Then, a third term is included in the summation in Eq. (5).

In the modeling we take into account experimental errors in incident angle and angular spread due to the substrate design, and film thickness nonuniformity. It is difficult to model both the thickness and the dielectric properties simultaneously in ellipsometry.[45,46] Thus, we allow the layer thicknesses to vary only slightly around our measured thickness values during fitting. The output from the modeling consists of the best-fit value of the Lorentz-Drude parameters [see Eq. (6)] and their 90% confidence intervals.

2. Optical constants of the glass substrate

The optical constants of the quartz substrates (both flat and semicylindrical) and the quartz window used in the optical gas loading cell (see Fig. 2) are determined using optical reflection and transmission measurements and ellipsometry. This is straightforward, and our results match the tabulated values of the refractive index from the manufacturer as well as those of quartz glass cited in Ref. 59. The extinction coefficients are, however, not tabulated in Ref. 59. Our results on the extinction coefficient show a slight absorption near and above 6.5 eV, but still below 10^{-7}. The corresponding dielectric function is used in the consecutive modeling of the metal-hydride layers.

3. Optical properties of PdH_x

A 12-nm-thick Pd film, deposited on quartz is exposed to 1-bar hydrogen at RT in the optical gas loading cell and investigated in the ellipsometer (see Fig. 6 for the experimental and fitted data). The Pd hydride, PdH_x, that is formed is a strongly absorbing metal. Its dielectric function $\epsilon(\omega)=\epsilon_1+i\epsilon_2$ can be adequately parametrized with a Lorentz-Drude (LD) model:

$$\epsilon(\omega)=\epsilon_\infty-\sum_{i=1}^{N}\frac{\omega_{p,i}^2}{\omega^2+i\omega/\tau_i}+\sum_{j=1}^{M}\frac{f_j}{\omega_j^2-\omega^2-i\Gamma_j\omega}, \quad (6)$$

where the constant ϵ_∞ accounts for excitations far above 6.5 eV; the N Drude terms describe the free-carrier response with $\omega_{p,i}$ the plasma frequency of the ith Drude term and τ_i the relaxation time; the M Lorentz terms represent the effect of interband transitions with f_j the intensity of the jth oscillator, ω_j its energy, and Γ_j its broadening. The relation between the dielectric function and the refractive index n and extinction coefficient k is $\epsilon_1=n^2-k^2$ and $\epsilon_2=2nk$. The LD parameters obtained for PdH_x in 1-bar H_2 are given in Table I.

TABLE I. Lorentz-Drude parameters and their 90% confidence intervals of a 12-nm-thick PdH_x layer in 1-bar H_2 obtained from ellipsometric data (see Fig. 6). $\xi^2=7.4$ and $\epsilon_\infty=1.266\pm0.371$. All parameters are in eV.

i	$\omega_{p,i}$	$1/\tau_i$	j	ω_j	$\sqrt{f_j}$	Γ_j
1	3.389 ± 0.901	0.1892 ± 0.019				
2	8.656 ± 2.02	1.775 ± 0.147				
			1	3.418 ± 0.124	8.588 ± 4.6	5.195 ± 0.691
			2	6.878 ± 0.119	11.32 ± 4.63	7.713 ± 0.519
			3	9.669	11.96	0.5601

In addition to the sample for ellipsometry, an identical sample on a flat substrate is prepared for measurements in the spectrophotometer. The transmission and absolute reflection are determined for this sample in 40-mbar hydrogen (4% H_2 in Ar). It is not possible to use the optical gas loading cell when we determine the absolute reflection since we must look directly at the Pd sample and not via the substrate. To obtain a hydrogenated Pd sample, the whole spectrophotometer is purged in Ar containing 4% H_2, corresponding to a partial pressure of 40-mbar H_2. This is the highest H_2 concentration we can use in the (open) spectrophotometer. In Fig. 7 the experimental and fitted data are displayed, the LD parameters obtained for PdH_x in 40-mbar H_2 are given in Table II.

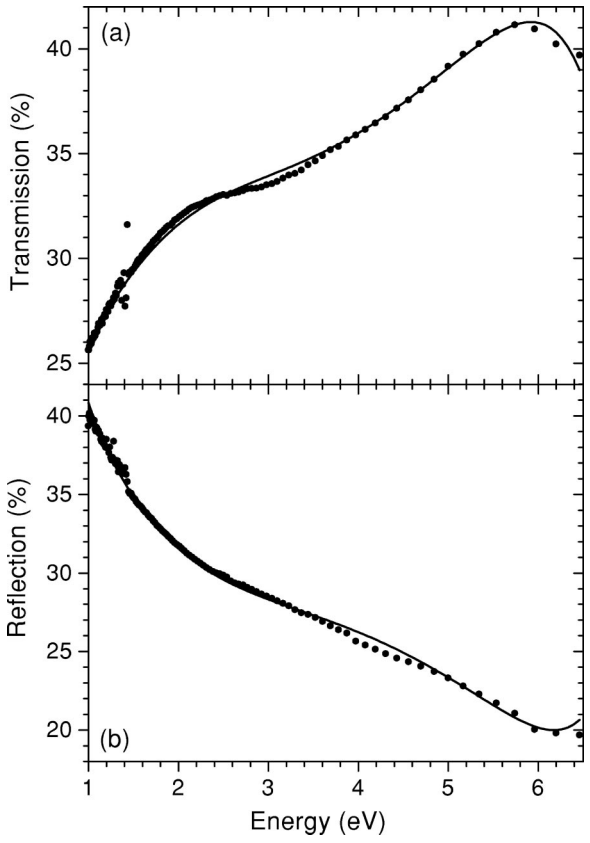

FIG. 7. Experimental and fitted transmission (a) and reflection (b) data for a 12-nm-thick Pd film in 40-mbar H_2 (4% H in Ar) used to determine the dielectric function of PdH_x (see Fig. 8). The mean-squared error corresponding to the fit is 1.04.

The difference in ξ^2 (see Tables I and II) between the 1-bar and 40-mbar measurements is mainly due to the different substrate geometry, semicylindrical vs flat substrate. We assign the major part of this difference in ξ^2 to the cylindrical incident and exit surface of the semicylindrical substrate and to the fact that the ellipsometry measurements have been performed from the ''backside'' of the sample through the substrate. Note that this does not change the dielectric function, it merely gives a larger spread in the input data for the analysis.

In Fig. 8 we show the resulting dielectric function at 1-bar and 40-mbar H_2 partial hydrogen pressure, and compare it to literature data for PdH_x by von Rottkay *et al.*[60] and literature data for Pd from Ref. 59.

The plasma frequency ω_p of PdH_x in 1-bar H_2 is slightly larger than the one in 40-mbar H_2. Because $\omega_p\propto\sqrt{n_c}$ with n_c the charge-carrier density, there are more free charge carriers in PdH_x in 1-bar than in 40-mbar H_2. Values for the (optical) resistivity $\rho_{\rm opt}$ can be derived from the Drude parameters using

$$\rho_{\rm opt}=\frac{1}{\epsilon_0\omega_p^2\tau}, \tag{7}$$

with ϵ_0 the vacuum permittivity, ω_p is the plasma frequency, and τ is the electron relaxation time. This optical resistivity calculated for the dominant Drude term $i=2$ shows the same trend as the plasma frequency itself: In 40-mbar H_2, PdH_x has a resistivity of 235 $\mu\Omega$ cm, in 1 bar 178 $\mu\Omega$ cm. However, bulk Pd has a resistivity of 10.53 $\mu\Omega$ cm and PdH_x has a maximum resisitivity of about 20 $\mu\Omega$ cm when $x=0.7$ at RT.[61] Our much larger resistivities are probably due to the fact that the 12-nm-thick Pd film consists of somewhat disconnected islands. Hydrogen absorption causes the Pd islands to expand which decreases the resistivity between them.[62,63] Thus, we have a sort of percolation effect and the resistivity is lower in 1-bar H_2 than in 40-mbar H_2 contrary to bulk PdH_x.

4. Optical constants of the double layer Pd/Mg

To investigate the optical properties of the partially interdiffused Pd-Mg top layer, we deposit a layer of 10-nm Mg capped with 10-nm Pd on quartz. This Pd-Mg film is then exposed to hydrogen at 100 °C and 100 bar [together with the thick Mg film covered by Pd (see Fig. 1)]. After hydrogenation the optical properties are determined in the optical

TABLE II. Lorentz-Drude parameters and their 90% confidence intervals of a 12-nm-thick PdH_x layer in 40-mbar H_2 (4% H_2 in Ar) obtained from reflection and transmission data (see Fig. 7). $\xi^2=1.04$, and $\epsilon_\infty = 1.280 \pm 0.241$. All parameters are in eV.

i	$\omega_{p,i}$	$1/\tau_i$	j	ω_j	$\sqrt{f_j}$	Γ_j
1	5.156 ± 0.955	0.001 ± 0.0241				
2	8.382 ± 2.65	2.238 ± 0.323				
			1	4.131 ± 0.111	9.815 ± 4.17	7.104 ± 0.581
			2	7.623 ± 0.249	7.793 ± 4.14	0.927 ± 0.235

gas loading cell at RT. This sample is treated as consisting of two layers: a Mg-rich Pd-Mg alloy on the substrate covered with a Pd-rich Pd-Mg alloy on top. As starting values for the fitting procedure we use the PdH_x dielectric function determined above for the Pd-rich Pd-Mg top layer, and combine it with voids in a Bruggeman effective medium approximation to take surface roughness into account.[64] A Lorentz-Drude model is used for the second layer, the Mg-rich Pd-Mg alloy. Ellipsometric data for three angles of incidence (55, 60, and 65°) and normal incidence transmission data are then combined in a multiple data type fit. All data are measured on the same sample and during fitting the layer optical functions and thicknesses are coupled. The final iteration results in a fit with a ξ^2 of 8.7. The optical properties of this double layer are then used as starting values for the top layer of the thicker MgH_2 film.

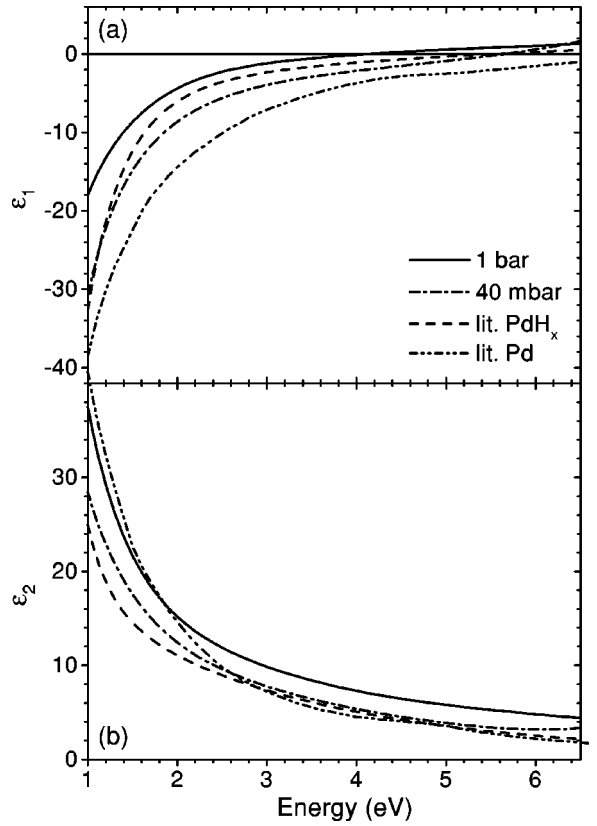

FIG. 8. Real (a) and imaginary (b) parts of $\epsilon(\omega)$ for the PdH_x films as determined from ellipsometry in 1-bar H_2 (see Fig. 6) and reflection and transmission measurements in 40-mbar H_2 (4% H_2 in Ar) (see Fig. 7). For comparison, the dielectric function found by von Rottkay *et al.* (Ref. 60) for PdH_x in 4% H_2 and the dielectric function of pure Pd according to Ref. 59 are included.

5. Dielectric function of MgH_2

In the evaluation of the optical properties of MgH_2 we analyze ellipsometric and transmission data of a 124-nm-thick MgH_2 film capped with 12-nm PdH_x (as measured with a mechanical stylus profilometer in the hydrogenated state). In addition to these data, transmission data of a compositionally identical film, but with a thickness of 162 nm (when hydrogenated) are included in the modeling. These three datasets are evaluated in three parallel, coupled models simultaneously. The main features can be modeled using two Lorentz oscillators at the high-energy side of the measured spectra at 6.4 and 6.9 eV. These oscillators mark the beginning of the conduction band.

The optical parameters of the capping layer, consisting of the Pd-rich Pd-Mg alloy on top of the Mg-rich Pd-Mg alloy, are initially fixed to the parameter values obtained in Sec. III C 4. The only parameters of the top layers which are allowed to vary are the thicknesses since the diffusion of Pd into MgH_2 may be larger than the 10 nm in the thin Pd/Mg double layer. In the final iteration a global fit is used in which all LD parameters are allowed to change. The final ξ^2 is 17.17. Table III gives the LD parameter values from the final iteration for MgH_2, the Pd-rich Pd-Mg cap layer and the Mg-rich Pd-Mg cap layer.

The plasma frequencies obtained for the two top layers give us a clue about their composition. Since the plasma frequency of the top layer ($\omega_p = 14.35$ eV) is much larger than the one of the lower cap layer ($\omega_p = 6.672$ eV), the top layer has a larger charge-carrier density and is thus more metallic than the lower one. This indicates that the top layer is formed by a *metallic* Pd-Mg alloy. The lower layer contains some insulating MgH_2 as well. The optical resistivity [see Eq. (7)] of the top layer is 38 $\mu\Omega$ cm compared to an electrical resistivity of 630 $\mu\Omega$ cm (at RT) for the total stack as measured after loading. Thus, the top layer is indeed shunting the resistivity measurements of MgH_2. Since PdH_x has an optical resistivity of 178 $\mu\Omega$ cm it is clear that the top layer contains some metallic Mg as well which has a much lower resistivity (6.5 $\mu\Omega$ cm).

The total thickness of the stack obtained from ellipsometry is 130.6 nm after hydrogenation. With the stylus pro-

TABLE III. Lorentz-Drude parameters and their 90% confidence intervals of a 124-nm MgH_2 film covered with 12-nm Pd obtained from ellipsometric and transmission data (see Fig. 9). $\xi^2=17.17$ and $\epsilon_\infty=1.595\pm0.092$. All parameters are in eV.

i	$\omega_{p,i}$	$1/\tau_i$	j	ω_j	$\sqrt{f_j}$	Γ_j
			MgH_2 film, $d=115.9$ nm			
			1	6.4	5.516	0.6454
			2	6.9	7.689 ± 0.519	0.01223 ± 0.109
			Top cap layer: Pd-rich Pd-Mg alloy (with 53% voids), $d=15.6$ nm			
			1	2.964 ± 0.122	5.208 ± 0.559	1.702 ± 9.03
			2	8.5	17.408 ± 12.2	0.01366 ± 4.96
			Lower cap layer: Mg-rich Pd-Mg alloy, $d=4.1$ nm			
1	6.672 ± 0.865	0.003629 ± 8.29				
			1	3.293 ± 0.0824	24.61 ± 0.420	14.09 ± 7.06

filometer we found a thickness of 136 nm. However, as mentioned before the profilometer gives a value that is too large. Before hydrogenation the thickness was 95 nm. This would mean an increase of 37.5% instead of the theoretical 32% volume expansion.

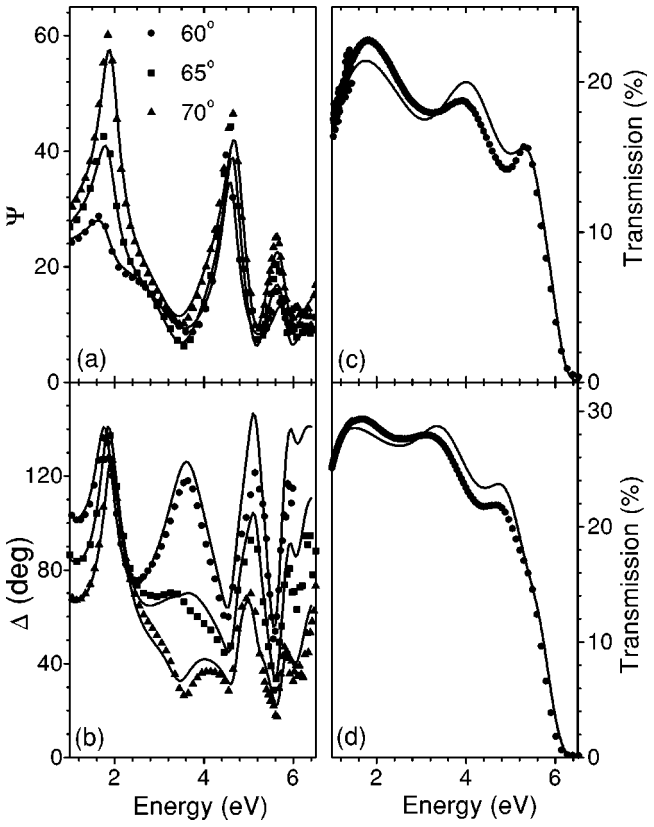

FIG. 9. Experimental and fitted data for a 124-nm-thick MgH_2 film covered with 12-nm Pd used to determine the dielectric function of MgH_2 (see Fig. 10); (a) ellipsometric data for Ψ, (b) ellipsometric data for Δ, (c) optical transmission, (d) transmission of a sample consisting of 150-nm MgH_2/12-nm Pd. All experimental data are modeled simultaneously in the fitting procedure as described in Sec. III C. The mean-squared error of the fit is 17.17.

In Figs. 9(a) and 9(b) the experimental and fitted values of Ψ and Δ are given, in (c) and (d) the experimental and fitted transmission curves are shown. Finally, Fig. 10(a) and 10(b) show the real and imaginary part of $\epsilon(\omega)$ obtained for α-MgH_2.

IV. DISCUSSION

In Table IV both experimental and theoretical values for the band gap of MgH_2 are given. Hartree-Fock calculations are not included since this method overestimates the band gap considerably. Very recent and not yet published theoretical work by Herzig,[68] Auluck,[69] and Alford and Chou[70] on MgH_2 is included.

The band gap of 5.6 ± 0.1 eV determined in this work for α-MgH_2 is close to values mentioned in literature. A gap of 5.16 eV was obtained in an UV-absorption study mentioned by Krasko.[14] However, details about how this value was obtained have never been published. The value found by He and Pong[15] for the average band gap $\langle E_g\rangle$ is close to ours. This is rather surprising since $\langle E_g\rangle$ was obtained in an indirect way from x-ray photoelectron spectroscopy (XPS) data using Penn's formula.[16] Yamamoto *et al.*[17] measured the specular optical transmission of thin layers of MgH_2 covered by Pd and found that the transmission is zero at 6.05 eV. However, they did not apply Tauc's method (see Sec. III B) to the transmission edge in order to obtain an estimate for the band gap. Furthermore, one should keep in mind that 6.05 eV is at the detection limit of their Shimadzu spectrophotometer.

As can be seen in Table IV LDA calculations give a band gap that is systematically too low. This is a well-known feature of this approximation. Similarly, the GGA used in two other papers[8,13] to calculate the density of states of MgH_2, underestimates the band gap. Our band gap is closest to the theoretically calculated gaps of Herzig[68] using screened-exchange–LDA (sX-LDA) and Alford and Chou[70] using the GW approximation (GWA). Furthermore, it is interesting to point out that our experimentally found gap $E_g=5.6\pm0.1$ eV is very close to the difference in ionization energy between Mg and H: 5.952 eV.

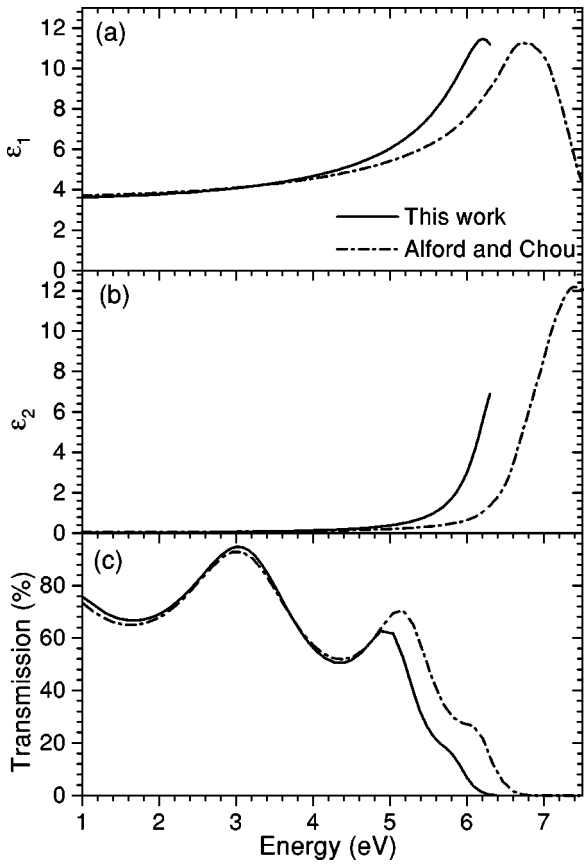

FIG. 10. Real (a) and imaginary (b) parts of $\epsilon(\omega)$ for MgH_2 determined from ellipsometry and transmission data (see Fig. 9). The real and imaginary parts calculated by Alford and Chou (Ref. 70) using the GW approximation are shown for comparison. The transmission of a 100-nm MgH_2 film in vacuum calculated with the dielectric functions shown in (a) and (b) is displayed in the lower panel (c). The theoretical gap is ≈ 0.5 eV too large.

Back in 1955 Ellinger *et al.*[18] determined the refractive index of α-MgH_2 at 589.3 nm (2.107 eV) and found $n=1.95$ and 1.96 for the ordinary and extraordinary rays, respectively. We find $n=1.94$ and $k=7.6\times10^{-3}$ at the same energy which is very close.

Both Auluck[69] using LDA and Alford and Chou[70] using LDA and GWA have calculated the band structure and dielectric function for α-MgH_2. To obtain the dielectric function only direct transitions are taken into account. The only difference between the LDA and GWA curves is the energy position. The dielectric function obtained for α-MgH_2 with GWA agrees quite well with our measured values [see Figs. 10(a,b)], while the LDA curve, as expected, is shifted to too low energies. This indicates that a scissors operation that shifts the conduction band rigidly with respect to the valence band works well to correct LDA calculations.[71,72] The energy at which both ϵ_1 and ϵ_2 exhibit a marked increase is, however, slightly different for the experiment and the GWA calculation. sX-LDA seems to overestimate the band gap since it gives even larger values for the (in)direct gap than GWA.

Figure 10(c) shows the optical transmission for a 100-nm-thick MgH_2 film in vacuum as calculated with our experimental dielectric function and the one calculated by Alford and Chou. As can be seen MgH_2 has an intrinsic transparency of about 80% over the entire visible spectrum. The difference in energy between the absorption edges of the two transmission spectra and the dielectric functions is about 0.5 eV. Thus, GWA overestimates the optical gap by 0.5 eV. The direct gap determined from the band structure using GWA is 6.11 eV. Subtracting 0.5 eV from 6.11 eV gives a value of 5.61 eV which is within the error margin of our experimentally found gap. More information about the dielectric function and band structure of MgH_2 by Alford and Chou will be published elsewhere.

Yet unpublished calculations indicate that the optical properties of both α- and γ-MgH_2 are close to each other.[69,70] Vajeeston *et al.*[8] find a gap of 4.2 and 4.3 eV for α- and γ-MgH_2, respectively, with GGA; Bastide *et al.*[9] and Bortz *et al.*[10] have found that the structures of the two different phases are closely related and that the density is almost the same as well as the H-H distances. Therefore, our dielectric function for α-MgH_2 is probably a very good approximation for γ-MgH_2 as well. This is important to model the optical properties of switchable mirrors since in fully hydrogenated Y-Mg alloys Nagengast *et al.* found that fcc YH_3 coexists with γ-MgH_2.[27] β-MgH_2 seems to be very different both structurally[9] and optically. Its density is much larger and the calculated band gap for this material turns out to be considerably smaller than that of both α- and γ-MgH_2

TABLE IV. Literature data for the band gap E_g of MgH_2 both experimental (expt.) and calculated (calc.). In parentheses the smallest direct gap for MgH_2 is given. (EELS is electron-energy-loss spectroscopy.)

Material		Method	E_g (eV)	Reference
α-MgH_2	expt.	UV absorption	5.16	14
		XPS	5.8	15
		EELS	>3.7 [a]	65
		XPS	>3.4 [a]	66
		Transmission	6.05 [b]	17
		Ellipsometry/ Transmission	5.6 ± 0.1	this work
	calc.	LDA	3.06	11
		LDA	3.4	12
		LDA	3.45 (4.34)	68
		LDA	3.3	69
		LDA	3.10	70
		GGA	3.78	13
		GGA	4.2	8
		sX-LDA	5.71 (6.41)	68
		GWA	5.25 (6.11)	70
γ-MgH_2	calc.	GGA	4.3	8
β-MgH_2	calc.	APW	0.23	67
		GGA	2.35	73

[a]If there are no charging effects, the band gap would be twice the indicated value.

[b]This is the photon energy where the transmission vanishes.

TABLE V. Literature data for the band gap E_g of materials closely related to MgH_2 both experimental (expt.) and calculated (calc.). (PES stands for photoemission spectroscopy.)

Material		Method	E_g (eV)	Reference
MgF_2	expt.	Reflectance	12.4	74
	calc.	tight binding, pseudopotentials	12.8	75
MgO	expt.	Reflectance	7.77	76
	calc.	LDA	~ 5	77
		GWA	7.8	77,82
MgS	calc.	LDA	2.6	84
		LDA (corrected)	4.59	78
MgSe	expt.		5.6	79
MgTe	expt.		4.7, 3.6	79
CaH_2	expt.	XPS	~ 5[a]	87
		PES	~ 5[a]	80
	calc.	LDA	3.32	83
SrH_2	expt.	XPS	~ 5[a]	87
BaH_2	expt.	XPS	~ 5[a]	87
		XPS	>2.2[b]	66
LiH	expt.		4.99	81
	calc.	GWA	5.24	81
LiD	expt.		5.04	82
	calc.	LDA	2.84	82
		GWA	5.37	82

[a]Charging effects are taking into account in the experiments.

[b]If there are no charging effects, the band gap would be twice as large.

(see Table IV). Augmented plane-wave (APW) calculations underestimate the band gap considerably, the GGA value of 2.35 eV (again by Vajeeston[73]) is much more reliable. The difference between the calculated band gap using GGA (Ref. 8) and the one measured for α-MgH_2 is 1.4 eV. Assuming that the same scissors operation can be applied to γ-MgH_2 (Ref. 8) and β-MgH_2 (Ref. 73) we expect an experimental gap of 5.7 eV for γ-MgH_2 and 3.75 eV for β-MgH_2.

We now compare MgH_2 to related materials such as MgF_2, MgO, MgS, MgSe, and other alkaline-earth and alkali metal hydrides. In Table V the band gaps of these materials are listed. For all of them it turns out that LDA underestimates the measured gap. Again, as for MgH_2, the GW approximation seems to give a very good agreement between experiment and calculation for MgO, LiH, and LiD. The same is true for the alkali metal halides.[82] MgH_2 and CaH_2 seem to be very similar. Both materials are wide band-gap insulators and have a valence band that is predominantly determined by hydrogen orbitals.[11,12,83] For MgO and MgS both valence and conduction bands are determined by the anions (O or S)[84] as well and again the same holds for the alkali metal halides.[85]

Since both the valence and conduction band of MgH_2 are formed by H states, the band gap of the alkaline-earth hydrides is expected to be almost independent of the metal as is the case for the alkali metal halides.[85,86] The remaining dependence results from the influence of the metal ion on the lattice parameter and the influence of hybridization of the conduction band states with metal-ion *s* and *d* states. From XPS experiments by Franzen *et al.*[87] it seems that the onset of transitions in the valence-band regions start for CaH_2, SrH_2, and BaH_2 all at about 2.5 eV. Since charging effects are taking into account, this gives a gap of about 5 eV quite close to what we have found for α-MgH_2. It is striking that LiH and LiD also have a gap of 5.0 eV.

V. CONCLUSIONS

In this study we use a special experimental setup for optical transmission and ellipsometry measurements. This setup facilitates greatly measurements of the optical properties and dielectric function of metal hydrides in a hydrogen environment. It is possible to control the gas pressure from 1 mbar to 100 bar, and thus the composition of metal hydrides over a wide range. The temperature, pressure, and resistivity are monitored *in situ* during hydrogenation of a sample. We determine the dielectric properties of α-MgH_2 and PdH_x and find that MgH_2 is a transparent, color neutral insulator with a band gap of 5.6 ± 0.1 eV. The transparency over the whole visible spectrum is $\sim 80\%$ (for a 100-nm-thick film). The experimentally determined dielectric function in the photon energy range between 1 and 6.5 eV of α-MgH_2 is in very good agreement with very recent calculations using the GW approximation. If we assume that calculations of the band gap for γ- and β-MgH_2 underestimate the experimental gap by the same amount as in α-MgH_2 we expect an experimental gap of 5.7 eV for γ-MgH_2, and 3.75 eV for β-MgH_2.

In a coming publication we shall show that the dielectric function of MgH_2 determined here can be used to explain the large optical absorption (the so-called ''black state'') of Mg-based alloys where metallic Mg and insulating MgH_2 nanodomains coexist.

ACKNOWLEDGMENTS

The authors would like to thank N. J. Koeman, J. H. Rector, and W. Lohstroh for their valuable help with the deposition and characterization of the samples. L. Jansen is gratefully acknowledged for constructing the optical gas loading cell and high pressure loading chamber. We are also very grateful to J. A. Alford, M. Y. Chou, P. Herzig, S. Auluck, and P. Vajeeston for making available to us the results of their band-structure calculations before publication. This work is part of the research program of the Stichting voor Fundamenteel Onderzoek der Materie (FOM), financially supported by the Nederlandse Organisatie voor Wetenschappelijk Onderzoek (NWO).

*Present address: Solid State Physics, Uppsala University, Box 534, SE-751 21 Uppsala, Sweden.

†Corresponding author. Electronic address: giebels@nat.vu.nl

[1] H. Kohlmann, *Encyclopedia of Physical Sciences and Technology*, 3rd ed. (Academic Press, New York, 2002), Vol. 9, p. 441.

[2] L. Schlapbach and A. Züttel, Nature (London) **414**, 353 (2001).

[3] P. Selvam, B. Viswanathan, C.S. Swamy, and V. Srinivasan, Int. J. Hydrogen Energy **11**, 169 (1986).

[4] A. Zaluska, L. Zaluski, and J.O. Ström-Olsen, J. Alloys Compd. **288**, 217 (1999).

[5] G. Liang, J. Huot, S. Boily, A. Van Neste, and R. Schulz, J. Alloys Compd. **292**, 247 (1999).

[6] Z. Dehouche, R. Djaozandry, J. Huot, S. Boily, J. Goyette, T.K. Bose, and R. Schulz, J. Alloys Compd. **305**, 264 (2000).

[7] J.F. Pelletier, J. Huot, M. Sutton, R. Schulz, A.R. Sandy, L.B. Lurio, and S.G.J. Mochrie, Phys. Rev. B **63**, 052103 (2001).

[8] P. Vajeeston, P. Ravindran, A. Kjekshus, and H. Fjellvåg, Phys. Rev. Lett. **89**, 175506 (2002).

[9] J.P. Bastide, B. Bonnetot, J.M. Létoffé, and P. Claudy, Mater. Res. Bull. **15**, 1215 (1980).

[10] M. Bortz, B. Bertheville, G. Böttger, and K. Yvon, J. Alloys Compd. **287**, L4 (1999).

[11] R. Yu and P.K. Lam, Phys. Rev. B **37**, 8730 (1988).

[12] B. Pfrommer, C. Elsässer, and M. Fähnle, Phys. Rev. B **50**, 5089 (1994).

[13] U. Häussermann, H. Blomqvist, and D. Noréus, Inorg. Chem. **41**, 3684 (2002).

[14] G. Krasko, *Metal-Hydrogen Systems* (Pergamon, New York, 1982), p. 367.

[15] Z.X. He and W. Pong, Phys. Scr. **T41**, 930 (1990).

[16] D.R. Penn, Phys. Rev. **128**, 2093 (1962).

[17] K. Yamamoto, K. Higuchi, H. Kajioka, H. Sumida, S. Orimo, and H. Fujii, J. Alloys Compd. **330-332**, 352 (2002).

[18] F.H. Ellinger, J.C.E. Holley, B.B. McInteer, D. Pavone, R.M. Potter, E. Staritzky, and W.H. Zachariasen, J. Am. Chem. Soc. **77**, 2647 (1955).

[19] J.N. Huiberts, R. Griessen, J.H. Rector, R.J. Wijngaarden, J.P. Dekker, D.G. de Groot, and N.J. Koeman, Nature (London) **380**, 231 (1996).

[20] P.H.L. Notten, M. Kremers, and R. Griessen, J. Electrochem. Soc. **143**, 3348 (1996).

[21] E.S. Kooij, A.T.M. van Gogh, and R. Griessen, J. Electrochem. Soc. **146**, 2990 (1999).

[22] P. van der Sluis, M. Ouwerkerk, and P.A. Duine, Appl. Phys. Lett. **70**, 3356 (1997).

[23] T.J. Richardson, J.L. Slack, R.D. Armitage, R. Kostecki, B. Farangis, and M.D. Rubin, Appl. Phys. Lett. **78**, 3047 (2001).

[24] J. Isidorsson, I.A.M.E. Giebels, E.S. Kooij, N.J. Koeman, J.H. Rector, A.T.M. van Gogh, and R. Griessen, Electrochim. Acta **46**, 2179 (2001).

[25] S.J. van der Molen, D.G. Nagengast, A.T.M. van Gogh, J. Kalkman, E.S. Kooij, J.H. Rector, and R. Griessen, Phys. Rev. B **63**, 235116 (2001).

[26] J. Isidorsson, I.A.M.E. Giebels, M. Di Vece, and R. Griessen, Proc. SPIE **4458**, 128 (2001).

[27] D.G. Nagengast, A.T.M. van Gogh, E.S. Kooij, B. Dam, and R. Griessen, Appl. Phys. Lett. **75**, 2050 (1999).

[28] M. Di Vece, S.J.M. Zevenhuizen, and J.J. Kelly, Appl. Phys. Lett. **81**, 1213 (2002).

[29] M. Di Vece, A.M.J. van der Eerden, J.A. van Bokhoven, S. Lemaux, J.J. Kelly, and D.C. Koningsberger, Phys. Rev. B **67**, 035430 (2003).

[30] B. Darriet, M. Pezat, A. Hbika, and P. Hagenmuller, Int. J. Hydrogen Energy **5**, 173 (1980).

[31] D. Sun, F. Gingl, Y. Nakamura, H. Enoki, M. Bououdina, and E. Akiba, J. Alloys Compd. **333**, 103 (2002).

[32] I.A.M.E. Giebels, J. Isidorsson, E.S. Kooij, A. Remhof, N.J. Koeman, J.H. Rector, A.T.M. van Gogh, and R. Griessen, J. Alloys Compd. **330-332**, 875 (2002).

[33] R. Griessen, Phys. Bl. **53**, 1207 (1997).

[34] I. A. M. E. Giebels, J. Isidorsson, and R. Griessen (unpublished).

[35] J. Isidorsson, I.A.M.E. Giebels, R. Griessen, and M. Di Vece, Appl. Phys. Lett. **80**, 2305 (2002).

[36] A. Krozer and B. Kasemo, J. Vac. Sci. Technol. A **5**, 1003 (1987).

[37] A. Krozer and B. Kasemo, J. Phys.: Condens. Matter **1**, 1533 (1989).

[38] J. Rydén, B. Hjörvarsson, T. Ericsson, E. Karlsson, A. Krozer, and B. Kasemo, J. Less-Common Met. **152**, 295 (1989).

[39] A. Krozer and B. Kasemo, J. Less-Common Met. **160**, 323 (1990).

[40] P. Spatz, H.A. Aebischer, A. Krozer, and L. Schlapbach, Z. Phys. Chem. (Munich) **181**, 393 (1993).

[41] Z. Luz, J. Genossar, and P.S. Rudman, J. Less-Common Met. **73**, 113 (1980).

[42] R. J. Westerwaal, I. A. M. E. Giebels, N. J. Koeman, and R. Griessen (unpublished).

[43] L.J. van der Pauw, Philips Res. Rep. **13**, 1 (1958).

[44] R. M. A. Azzam and N. M. Bashara, *Ellipsometry and Polarized Light* (North-Holland, Amsterdam, 1977).

[45] W.A. McGahan, B. Johs, and J.A. Woollam, Thin Solid Films **234**, 443 (1993).

[46] K. Järrendahl and H. Arwin, Thin Solid Films **313-314**, 114 (1998).

[47] P. Hjort, A. Krozer, and B. Kasemo, J. Alloys Compd. **234**, L11 (1996).
[48] *Handbook of Chemistry and Physics*, 82nd ed., edited by D. R. Lide (CRC Press, Cleveland, 2001).
[49] A. Fischer, H. Köstler, and L. Schlapbach, J. Less-Common Met. **172-174**, 808 (1991).
[50] S.J. van der Molen, J.W.J. Kerssemakers, J.H. Rector, N.J. Koeman, B. Dam, and R. Griessen, J. Appl. Phys. **86**, 6107 (1999).
[51] A. Borgschulte, M. Rode, A. Jacob, and J. Schoenes, J. Appl. Phys. **90**, 1147 (2001).
[52] T. Schober, Metall. Trans. A **12A**, 951 (1981).
[53] Lord Rayleigh, Philos. Mag. **41**, 274 (1871).
[54] J. Tauc, R. Grigorovici, and A. Vancu, Phys. Status Solidi **15**, 627 (1966).
[55] E. J. Johnson, *Absorption Near the Fundamental Edge*, Optical Properties of III-V Compounds of *Semiconductors and Semimetals*, Vol. 3 (Academic, New York, 1967), Chap. 6.
[56] G.E. Jellison, Jr., Appl. Opt. **30**, 3354 (1991).
[57] W. H. Press, B. P. Flannery, S. A. Teukosky, and W. T. Vetterling, *Numerical Recipes: the Art of Scientific Computing* (Cambridge University Press, Cambridge, MA, 1988).
[58] B.D. Johs, W.A. McGahan, and J.A. Woollam, Thin Solid Films **253**, 25 (1994).
[59] *Handbook of Optical Constants of Solids*, edited by E. D. Palik (Academic, San Diego, 1998).
[60] K. von Rottkay, M. Rubin, and P.A. Duine, J. Appl. Phys. **85**, 408 (1999).
[61] B.M. Geerken and R. Griessen, J. Phys. F: Met. Phys. **13**, 963 (1983).
[62] F. Favier, E.C. Walter, M.P. Zach, T. Benter, and R.M. Penner, Science **293**, 2227 (2001).
[63] O. Dankert and A. Pundt, Appl. Phys. Lett. **81**, 1618 (2002).
[64] D.E. Aspnes, J.B. Theeten, and F. Hottier, Phys. Rev. B **20**, 3292 (1979).
[65] P.T. Sprunger and E.W. Plummer, Chem. Phys. Lett. **187**, 559 (1991).
[66] A. Krozer, A. Fischer, and L. Schlapbach, Phys. Rev. B **53**, 13 808 (1996).
[67] M. Gupta, Z. Phys. Chem. (Munich) **181**, 543 (1993).
[68] P. Herzig (private communication).
[69] S. Auluck (private communication).
[70] J. A. Alford and M. Y. Chou (unpublished).
[71] F. Gygi and A. Baldereschi, Phys. Rev. Lett. **62**, 2160 (1989).
[72] R. Del Sole and R. Girlanda, Phys. Rev. B **48**, 11 789 (1993).
[73] P. Vajeeston (private communication).
[74] J. Thomas, G. Stephan, J.C. Lemonnier, M. Nisar, and S. Robin, Phys. Status Solidi B **56**, 163 (1973).
[75] C. Jouanin, J.P. Albert, and C. Gout, J. Phys. (Paris) **37**, 595 (1976).
[76] D.M. Roessler and W.C. Walker, Phys. Rev. **159**, 733 (1967).
[77] U. Schönberger and F. Aryasetiawan, Phys. Rev. B **52**, 8788 (1995).
[78] W.Y. Ching, F. Gan, and M.-Z. Huang, Phys. Rev. B **52**, 1596 (1995).
[79] W.H. Strehlow and E.L. Cook, J. Phys. Chem. Ref. Data **2**, 163 (1973).
[80] J.H. Weaver, M. Gupta, and D.T. Peterson, Solid State Commun. **51**, 805 (1984).
[81] S. Baroni, G.P. Parravicini, and G. Pezzica, Phys. Rev. B **32**, 4077 (1985).
[82] E.L. Shirley, Phys. Rev. B **58**, 9579 (1998).
[83] C.-Y. Xiao, J.-L. Yang, K.-M. Deng, Z.-H. Bian, and K.-L. Wang, J. Phys.: Condens. Matter **6**, 8539 (1994).
[84] P.K. de Boer and R.A. de Groot, J. Phys.: Condens. Matter **10**, 10241 (1998).
[85] P.K. de Boer and R.A. de Groot, Eur. Phys. J. B **4**, 25 (1998).
[86] F.C. Brown, C. Gähwiller, and H. Fujita, Phys. Rev. B **2**, 2126 (1970).
[87] H.F. Franzen, J. Merrick, M. Umaña, A.S. Khan, D.T. Peterson, J.R. McCreary, and R.J. Thorn, J. Electron Spectrosc. Relat. Phenom. **11**, 439 (1977).